Design and Analysis of a Valveless Impedance Pump for a Direct Sodium Borohydride–Hydrogen Peroxide Fuel Cell

A. S. Yang
Department of Energy and Refrigerating Air-Conditioning Engineering,
National Taipei University of Technology,
Taipei 515, Taiwan
e-mail: asyang@ntut.edu.tw

J. W. Tseng
Department of Aeronautics and Astronautics,
National Cheng Kung University,
Tainan 70101, Taiwan
e-mail: st88018@gmail.com

C. Y. Wen
Mem. ASME
Department of Mechanical Engineering,
The Hong Kong Polytechnic University,
Hung Hom, Kowloon, Hong Kong
e-mail: cywen@polyu.edu.hk

H. Zhang[1]
Department of Mechanical Engineering,
The Hong Kong Polytechnic University,
Hung Hom, Kowloon, Hong Kong
e-mail: 14900260r@connect.polyu.hk

A valveless impedance pump is designed and applied for the first time to supply the liquid fuels for a direct sodium borohydride–hydrogen peroxide fuel cell (DBHPFC). This valveless pump consists of an amber latex rubber tube, which is connected at both ends to rigid stainless-steel tubes of different acoustic impedance, and a simple actuation mechanism with a small direct control (DC) motor and a cam combined. The cam is activated by the motor and periodically compresses the elastic tube at a position asymmetrical from the tube ends. The traveling waves emitted from the compression combine with the reflected waves at the impedance-mismatched rubber tube/stainless-steel tube interfaces. The resulting wave interference creates a pressure gradient and generates a net flow. When connected to a DBHPFC with an active area of 25 cm^2, the pump can deliver the fuel at a maximum pumping rate of 30 ml/min, resulting in corresponding DBHPFC maximum power and a current of 13.0 W and 25.5 A, respectively. The specific power, volumetric power density, and back work ratio of the DBHPFC with this pumping method have been proven superior to those of the other pumping configuration with peristaltic pumps. This valveless impedance pump is mechanically simply and less susceptible to corrosion, and it can reduce the volume and weight of fuel cell systems to a measurable extent. The experimental results demonstrate the feasibility of the device for practical DBHPFC applications.
[DOI: 10.1115/1.4045703]

Keywords: impedance pump, valveless, direct sodium borohydride–hydrogen peroxide fuel cell, fuel cells

Introduction

Because of the general awareness of global warming in recent decades, fuel cells and other clean energy technologies have attracted considerable attention for many applications, including transportation, stationary power generation, and portable power electronics. Fuel cells can generate electricity with great efficiency and low levels of pollution and are on the brink of commercialization due to the availability and cost-competitiveness of practical system development.

The use of liquids as the fuel and oxidant for low-temperature fuel cells presents unique advantages over the conventional H_2/air fuel combination. Although an all-liquid fuel cell that uses water-based solutions in the fuel may introduce additional measures to manage water flow to avoid fuel solubility limits [1], it eliminates both membrane hydration and water blockage issues from gaseous H_2 fuel cells [2]. In addition, because the fuels used in all-liquid fuel cells are aqueous solutions that can also act as cooling media, the cooling plates integrated in the proton exchange membrane fuel cell stacks can be removed [3,4]. Of the various types of all-liquid fuel cells, direct sodium borohydride ($nabh_4$)–hydrogen peroxide (h_2o_2) fuel cells (DBHPFCs) have received increasing interest since the turn of the century as a potential high power source for mobile and portable applications [1,5–11]. When used directly as an anode fuel to power the DBHPFC, $NaBH_4$ provides greater electrochemical potential and reactivity than the use of gaseous hydrogen as the fuel. The discharge products of DBHPFC are water-soluble and environmentally benign. Moreover, $NaBH_4$ is a stable chemical reducing agent in dry air and has greater gravimetric hydrogen capacity than metal hydrides and greater volumetric hydrogen capacity than compressed and liquidized hydrogen. These characteristics make it easily storable and transportable and thus a good hydrogen storage material for fuel cell applications [11]. Combined with H_2O_2 as the cathode fuel, DBHPFCs have a theoretical open circuit voltage (OCV) of 2.24 V, via the following reactions [8], assuming that the oxidation of borohydride ions is straight and that no hydrogen intermediate formation occurs (Eq. (1)):

$$\text{Anode: } BH_4^- + 2H_2O = BO_2^- + 8H^+ + 8e^- E^0 = -0.471\,\text{V} \quad (1)$$

$$\text{Cathode: } H_2O_2 + 2H^+ + 2e^- = 2H_2O \quad E^0 = 1.77\,\text{V} \quad (2)$$

$$\text{Overall: } BH_4^- + 4H_2O_2 = BO_2^- + 6H_2O \quad E^0 = 2.24\,\text{V} \quad (3)$$

As shown in Eq. (1), 1 mol of borohydride releases 8 mol of electrons.

Nevertheless, BH_4^- is unstable in a neutral or acidic medium, so DBHPFCs work only in an alkaline environment. In addition, because a highly concentrated NaOH solution can inhibit the production of gaseous hydrogen from borohydride hydrolysis on the isolated catalyst particles, many researchers have used a borohydride fuel by dissolving $NaBH_4$ in an NaOH solution [7,9–11]. Similarly, on the cathode side, the use of acidified H_2O_2 as an oxidant in aqueous sulfuric acid (H_2SO_4) can inhibit oxygen generation and increase the output voltage of DBHPFC [6,9]. Because these aqueous anode and cathode fuels are generally circulated by pumps, the alkalinity of the BH_4^-/NaOH solution and the acidity of the H_2O_2/H_2SO_4 solution pose great challenges to the pump's anticorrosion requirement.

In general, mechanical pumps can be grouped into either displacement or dynamic types according to their operating

[1]Corresponding author.

Manuscript received April 13, 2019; final manuscript received November 4, 2019; published online December 13, 2019. Assoc. Editor: Bengt Sunden.

principles. Displacement pumps can be further classified as reciprocating (diaphragm) or peristaltic pumps. Reciprocating pumps incorporate a pressure chamber driven by an actuator and inlet and outlet passive check valves [12]. However, these moving valves make the pumps prone to mechanical failure and corrosion, which can further induce fluid leakage at high operating pressures and high levels of acidity/basicity accordingly. To resolve these problems, a variety of valveless peristaltic pumps have been adopted in DBHPFCs [5–9], but such systems generally have large volumes.

In the past two decades, a novel valveless scheme based on the impedance mismatch effect has been introduced in engineering applications [12–16]. This valveless impedance pump has a simpler structure and can generate a higher flowrate than the peristaltic schemes. As shown in Fig. 1, the valveless impedance pump typically consists of a flexible section connected at both ends to rigid sections of different acoustic impedance. The flexible section is compressed periodically at a location asymmetrical from the ends with various actuation mechanisms, including electric motors [12,16], electromagnetic actuators [13–15,17–21], and piezoelectric (PZT) actuators [22]. A pair of pressure waves is emitted in opposite directions each time the tube is compressed. These waves travel along the line and reflect when they reach the end of the line or the compression site if it is in the closed configuration. The traveling waves combine with the reflected waves at the impedance-mismatched positions, yielding wave interference and a pressure gradient accordingly. The resulting pressure gradient generates a net flow within the fluid system, which is typically pulsatile. The pumping rate is closely related to the combination of flexible and rigid materials (concerning impedance mismatch) and the compression parameters, such as the waveform, offset, compression amplitude, and duty cycle [23–32]. In general, the valveless impedance pump exhibits two distinct features: it responds in a nonlinear manner to the actuating compression frequency, and it reverses the flow direction at certain actuating frequencies and locations. In contrast, the peristaltic pump produces flow only in the direction of compression, and the flowrate varies in a linear manner with the actuation frequency. It is therefore essential to characterize the impedance pump and determine its optimal operational parameters (i.e., compression position, amplitude, and frequency) to generate the maximum flowrate for pumping fuels in the DBHPFC. Notably, because of the valveless and external compression features, the impedance pump and the peristaltic pump can both avoid the corrosion problem caused by the high acidity/basicity of the DBHPFC fuels.

In this study, a compact valveless impedance pump is designed, analyzed, and applied in a DBPHFC. Its commercial feasibility as a pump for high-performance DBPHFC systems is demonstrated.

Experiment

Valveless Impedance Pump. The impedance pump design of Wen et al. [16] was modified and further extended. As shown in Fig. 1, a circular amber latex rubber tube was chosen for the flexible section and two SS304 stainless-steel tubes were chosen for the rigid sections, because of their good anticorrosive characteristics in conditions of strong acidity and alkalinity. Meanwhile, the amber latex rubber tube possesses good wear-resistance and thermal aging characteristics. The length, outer diameter, and wall thickness of the rubber tube was 80 mm, 6 mm, and 1.0 mm, respectively. The stainless-steel tubes had a 0.5-mm wall thickness and an outer diameter of 5.0 mm. According to the earlier experimental studies of Wen et al. [16], actuating at $x/L = 1/8$ (see Fig. 1) and $\Delta y/D = 1$ (i.e., complete closure of the elastic tube) yields the maximum flowrate at any compression frequency f. A small direct control (DC) motor (FM-2088, Tricore Corp., Taiwan) was used to drive a cam and to compress the rubber tube at $x/L = 1/8$ and $\Delta y/D = 1$ at various f. The cam was made of lead solder because of its good lubrication characteristics under dry contact; its detailed dimensions are shown in the upper-right inset in Fig. 1. The corresponding duty cycle (i.e., the fraction of the time during which the cam is in contact with the elastic tube wall in an actuating period) is 36%. The dimensions of the motor are $16 \times 8 \times 6$ mm (length × width × height, respectively), and its power requirement is 1.5 W. Notably, the electromechanical compression mechanism used in our study offers a quiet, simple, economical, and low power consumption actuation to pump the fuels.

Direct Sodium Borohydride–Hydrogen Peroxide Fuel Cells. Figure 2 depicts the DBHPFC used in our research. A membrane electrode assembly (MEA, a CCM Nafion® 212 membrane with catalyst loading of anode and cathode: Pt 1.0 mg/cm^2 and Au 1.0 mg/cm^2, Yangtze Energy Technologies, Inc., Taiwan) sandwiched between two standard carbon cloths (W0S1002, CeTech, Co., Ltd., Taiwan) as gas diffusion layers was placed in the middle of two flow channel plates. The active area of MEA was 25 cm^2. The selection of Pt and Au as the catalysts for the anode and cathode, respectively, was based on the early experimental observations that a quasi-8e-reaction occurs at the Pt anode when an $NaBH_4$ alkaline solution (<1 M) was used as the anolyte [33] and that Au tends to minimize the decomposition of H_2O_2 [7]. Moreover, Au is resistant to corrosion and is easily applied. Both graphite bipolar plates ($80 \times 58 \times 4$ mm; Homytech, Taiwan) on the cathode and anode sides have three-parallel-channel serpentine flow fields, with channel widths and heights of 2 mm and 1 mm, respectively. The rib width is 1 mm. The DBHPFC was clamped between two aluminum alloy (6061T651) end plates

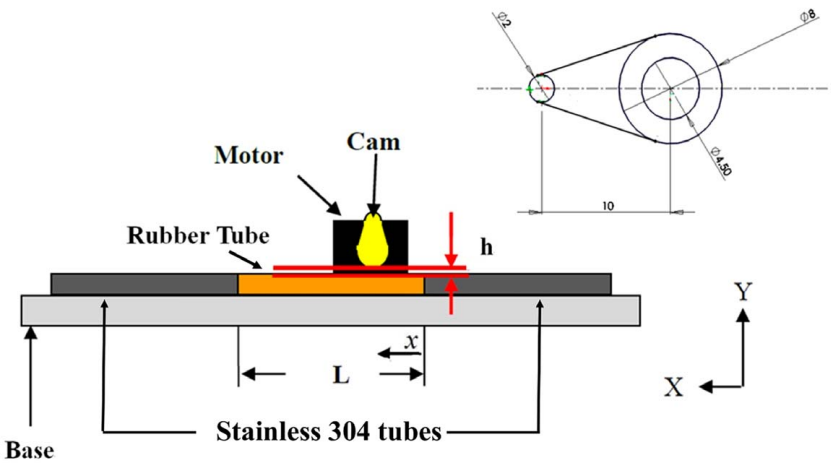

Fig. 1 Schematic of the impedance pump in the current study [12]

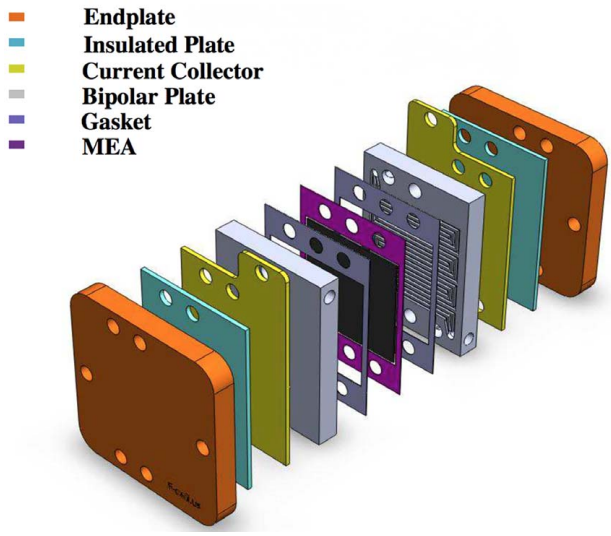

Fig. 2 Schematic of the DBHPFC6

(80 × 80 × 10 mm), with four bolts tightened with a uniform torque of 8 N m. Silica gel insulation plates (films) and copper current collectors were placed between the end plates and the cell. The DBHPFC temperature was controlled at 75 °C with two thin flexible heaters attached to end plates. The DBHPFC has no external thermal insulation.

Pump and Fuel Cell Performance Tests. Figure 3 illustrates the combined test scheme for the pumps and the fuel cell. The liquid fuels of the DBHPFC comprised an anode of an alkaline borohydride aqueous solution (5 wt% $NaBH_4$ and 15 wt% NaOH) and a cathode of an acidic hydrogen peroxide aqueous solution (2.0 M H_2O_2 + 1.0 M H_2SO_4). When pumped into the serpentine channels at the anode and cathode, respectively, the $NaBH_4$ and H_2O_2 solutions further diffused through the diffusion layers and then reacted under the anode and cathode catalysts. The heaters inside the polytetrafluoroethylene fuel tanks (500 ml each) heated both the anode and cathode electrolytes to 75 °C. This temperature was maintained with a control system using the proportional–integral–derivative (PID) control scheme; the temperatures of the fuels and the cell were tracked with K-type thermocouples.

A computer-controlled Arbin fuel cell test system (Arbin Instruments, BT2000, 1 kW), which comprises an electrical load and a data acquisition system, was used to control and record the current and voltage of the fuel cell unit under operation to obtain the *I–V* curves. With the DBHPFC connected to the electrical load, the *I–V* curves were measured in a constant-current model. The *I–V* curves of the DBHPFC pumped by peristaltic pumps (Great Tide Instrument Co., Ltd. Tp-100) and impedance pumps (as seen in Fig. 4) were compared. The impedance pumps shown in Fig. 4(*b*) are simple devices that are easily attached to the case wall of the entire fuel cell unit, which thus reduces the DBHPFC's operating weight and size.

As a preliminary step, the pumping performance of the impedance pump was calibrated both with and without the DBHPFC. As shown in Fig. 4(*b*), the pump alone (i.e., not connected to the DBHPFC) was connected to a fuel tank at one end, and the other end was left open to drain the fuel; this configuration was used to measure the flowrate profiles at various actuation frequencies. A DC power supply (MOTEH Co., Taiwan, LPS-305) was applied to an electric motor to drive the cam that compresses the elastic tube. The actuation voltage was monitored by a digital oscilloscope (Tektronix, TDS 2014). At the beginning of each experiment, the pump was filled with fuels. The correlation between the voltage applied to the motor, *V*, and the actuation frequency, *f*, under a load was initially calibrated with a stroboscope (Strobotac 1546). The pulse length of the flash is approximately 1.2 μs, which is short enough to freeze the motion of the cam as the correct flashing frequency is set. A linear regression analysis revealed a relationship between *f* and *V*: $f = 5\ V - 2$, for $11\ \text{V} \le V \le 15\ \text{V}$, with a high correlation coefficient (R^2 value of the fit) of 0.998.

The relevance of the pump flowrate to the actuation frequency was then measured. First, the fuel tank and the pump tubing were suffused with fuels and blocked with a ball valve at the end. To minimize the initial pressure head, the water level in the reservoir was 2.0 cm above the pump. The pump was then activated and the valve was opened. The fuel that exited from the fuel cell was collected in a

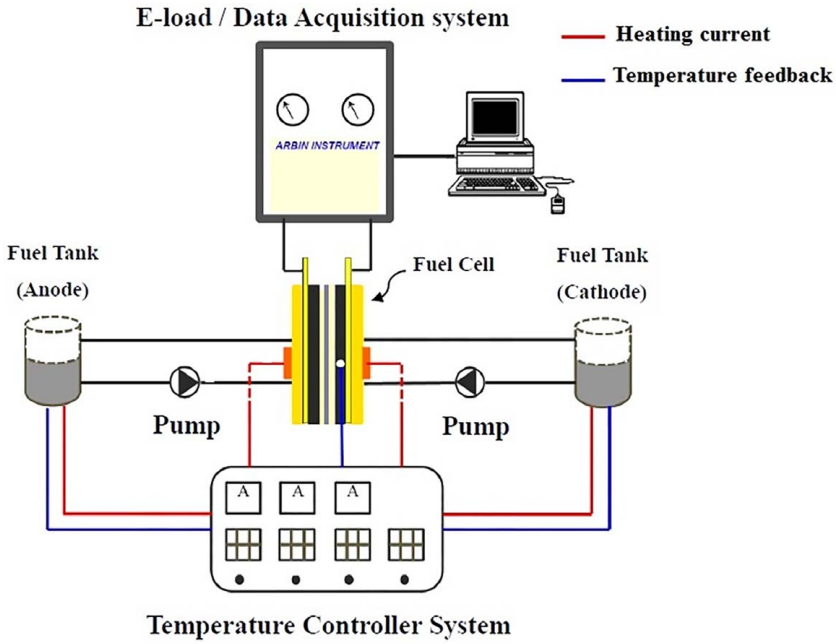

Fig. 3 Schematic of the performance test system for the DBHPFC connected with pumps

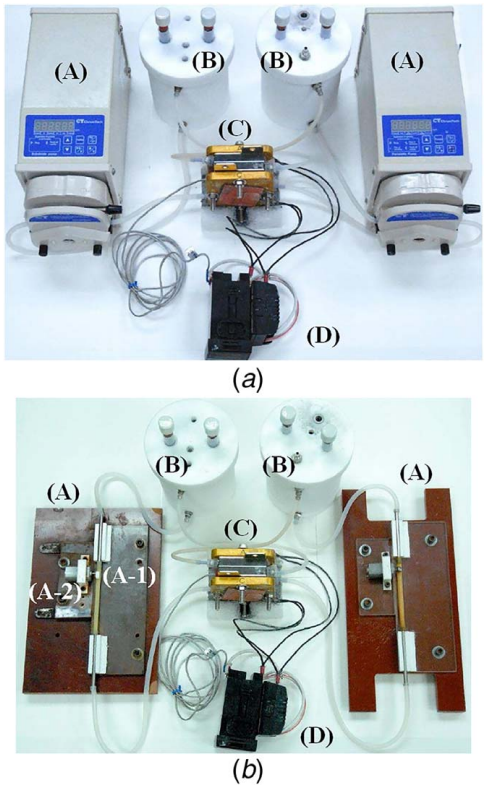

Fig. 4 Photos of the assembled DBHPFC test units pumped by (*a*) two peristaltic pumps and (*b*) two valveless impedance pumps: (*A*) pump, (*B*) fuel tank, (*C*) DBHPFC, (*D*) fuel cell heater power supply and temperature controller, (A-1) cam and (A-2) motor

sink for a few seconds to estimate the flowrate. The fuel flowrate was measured at every 1-V interval of the DC power supply change. Note that the ball valve and the sink are not shown in Fig. 4(*b*).

To obtain flowrate profiles for the pump with connection to the DBHPFC, the pump was connected to a fuel tank at one end and to the fuel cell at the other. The fuel flowrate was calculated by measuring the volume of fuel collected in the sink for a few seconds.

Results and Discussion

Effect of the Actuation Frequency on the Impedance Pump Flowrate. Figure 5 shows the measured impedance pump flowrates in response to the compression frequencies, actuating at $x/L = 1/8$ and $\Delta y/D = 1$ (complete closure of the elastic tube). The pump's performance was observed to depend in a nonlinear fashion on the actuation frequency for both the fuel cell-connected scenario (i.e., the dashed line in Fig. 5) and the pump alone (i.e., the solid line in Fig. 5). For the DBHPFC-connected scenario, the variation of the flowrate with the actuation frequency exhibited a broadly similar trend to that of the pump alone. No flow-reversal effect was induced beyond the limited applied frequency range. The unique frequency-dependence of the net flowrate indicates an impedance-driven flow. Note that the flowrate measurements have a very high degree of repeatability. For each experimental condition, 0.5% uncertainty was obtained via five repeated measurements for the flowrate. A maximum pump flowrate of $Q = 715$ ml/min was obtained for the pump alone scenario when the actuation force was applied at a frequency of 68 Hz (corresponding to an applied voltage of 14 V at the motor). Significant shrinkage of the flowrate at various compression frequencies was induced by the large head losses in the three-parallel-channel serpentine flow fields of the graphite bipolar plate. The maximum pump flowrate reduced to $Q = 30$ ml/min when the DBHPFC was connected to the impedance.

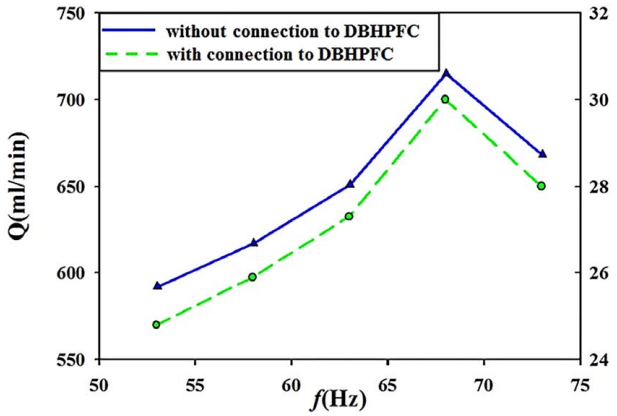

Fig. 5 Measured pump flowrates under different actuation frequencies with (right scale) and without (left scale) the DBHPFC connected. The actuation location is at $x/L = 1/8$ and $\Delta y/D = 1$.

As the working mechanism of the impedance pumps mentioned in the "Introduction section," a pair of pressure waves is emitted in opposite directions with each periodic compression of the tube. These waves travel along the tube and are then partially reflected when they reach the ends. The relative impedances of the two materials determine the proportion of the reflected wave energy to the total wave energy when they propagate through the intersection. The waves are delivered from a soft latex rubber tube to a very hard stainless-steel tube. The start time, travel distance, travel time, directions, amplitudes, and positions for each wave pair emitted are dependent upon the compression period and the cycle to which it belongs. Because the wave speed (estimated to be around 50–60 m/s [26]) in the latex rubber tube is much slower than the normal speed of sound (1500 m/s through water) inside the stainless-steel tubes, the pressure waves inside the pumping section that propagate to both ends are almost entirely reflected. As each wave crosses a reflection site, its pulse shape is reflected in a similar manner. All waves are eventually summed along the length of the compressed pliable tube. Once equilibrium is reached, a net pressure head is accordingly generated at the ends of the piping to impel the flow within the flow channel. The pump curve thus depends primarily upon the specific piping configuration and actuation parameters. Variations in the materials, the length of the pliable tube, the actuating wave pulse shapes, the actuating positions, and the actuating frequencies all affect the pump's performance [13]. Therefore, the head losses in the stainless-steel tube, bends, and the flow channel plate of the fuel cell system result in the nearly constant decrease of the flowrates in Fig. 5.

At an actuation frequency of 68 Hz and actuation position $x/L = 1/8$ (see Fig. 5), the total pump head is determined by $H_{pump} = Q_{pump} \times R_{pump} = Q_{fuelcell} \times (R_{pump} + R_{fuelcell})$, where Q_{pump} is the flowrate of the pump alone, Rpump is the internal pump flow resistance, $Q_{fuelcell}$ is the flowrate of the pump with connection to the DBHPFC, and $R_{fuelcell}$ is the total flow resistance of the stainless-steel tube, bends, and flow channel plate of the fuel cell system. Accordingly, the ratio of the total flow resistance of the fuel cell system to the internal pump flow resistance can be ascertained by $R_{fuelcell}/R_{pump} = Q_{pump}/Q_{fuelcell} - 1 = 715$ (ml/min)/30 (ml/min) $- 1 \approx 23$. Marked flow resistance of the flow channel plate emerged in the current study. To mitigate pressure head loss, the DBHPFC will require optimum flow channel plates for future practical applications.

Fuel Cell Performance Test. As illustrated in Fig. 6, this section focuses on performance testing of the fuel cell system, that is, the influence of the anode and cathode flowrates on the output power of the DBHPFC with the fuels, both oxidizer and reducing agents, circulated by the peristaltic pumps. Because the constant voltage of 0.7 V is close to the corresponding voltages at the maximum

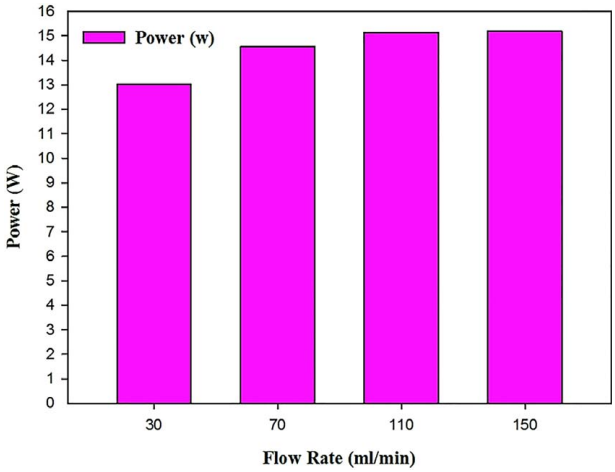

Fig. 6 Power performance of the DBHPFC at different flowrates

powers for all flowrates (see typical *I–V* curve in Fig. 7), the fuel cell power was measured while maintaining a constant voltage of 0.7 V. In addition, the flowrates were kept the same for the anode and the cathode, ranging from 30 to 150 ml/min with the increments of 40 ml/min. Note that increases in the anode and cathode flowrates gradually improve the DBHPFC performance. The measured output power was enhanced from 13 W (520 mW/cm^2) at 30 ml/min to 15.2 W (610 mW/cm^2) at 150 ml/min, but this increase stopped when the flowrates exceeded 110 ml/min. A further increase in the flowrates would increase the pumping power without accelerating fuel cell power generation. The current DBHPFC can achieve a maximum power density of 650 mW/cm^2, which is comparable to the value of 680 mW/cm^2 obtained by Gu et al. [9].

The fuel cell performance was further investigated by comparing two fuel pumping configurations at anode and cathode flowrates of 30 ml/min (i.e., the optimal flowrates for the current impedance pumps). Figure 7 shows the fuel cell *I–V* and power density curves using a pair of impedance pumps and a pair of peristaltic pumps (Fig. 4), respectively. Little disparity is observed in the DBHPFC performance between the two pumping mechanics. At anode and cathode flowrates of 30 ml/min, the DBHPFC has a maximum power density of about 530 mW/cm^2 and an OCV of 1.75 V.

Comparison of Pumping Efficiency. For quantitative evaluation of the performance of the DBHPFC with these two pumping

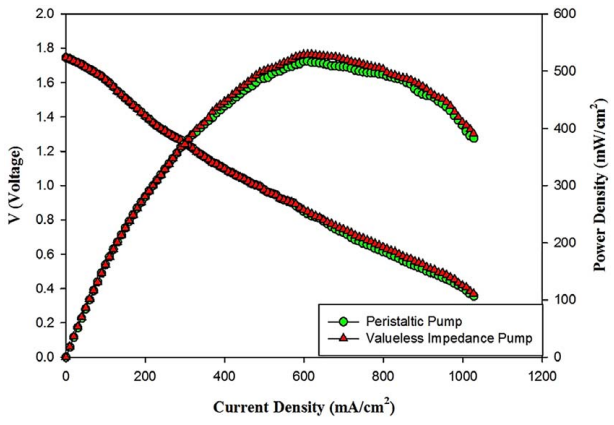

Fig. 7 *I–V* and power density characteristics when the DBHPFC is pumped by a pair of impedance pumps and a pair of the peristaltic pumps. The flowrates of both anode and cathode are 30 ml/min, corresponding to the optimal flowrate for the current impedance pump.

Table 1 A breakdown of the weight and volume for every component in the DBHPFC

Component	Weight (kg)	Volume (cm^3)
Impedance pump (×2)	4.33 (×2)	4331 (×2)
Peristaltic pump (×2)	0.039 (×2)	19
Fuel tank (×2)	1.52 (×2)	1505 (×2)
DBHPFC (×1)	0.078	150
Heater unit (×1)	0.4	400

Table 2 Comparison of the specific power, volumetric power density and back work ratio of the DBHPFC operated under two different pumping configurations with both anode and cathode flowrates of 30 ml/min

Configuration	Impedance pumps	Peristaltic pump
External power supplied (W)	1.5 (×2)	5 (×2)
Maximum power generated (W)	13.3	13.1
Mass of whole design (kg)	4.3	12.88
Volume of whole design (10^{-3} m^3)	7.23	12.37
Specific power (W/kg)	3.09	1.02
Volumetric power density (kW/m^3)	1.84	1.06
Back work ratio (%)	22.5	76.3

configurations, the specific power (power-to-mass ratio), volumetric power density, and back work ratio were defined as follows:

- Specific power $\equiv \frac{P_{produced}}{M_{total}}$
- Volumetric power density $\equiv \frac{P_{produced}}{V_{total}}$
- Back work ratio $\equiv \frac{P_{pumping}}{P_{produced}} \times 100\%$,

where $P_{produced}$, $P_{pumping}$, M_{total}, and V_{total} represent the maximum electrical power produced by the DBHPFC, the electrical power consumed by the pumps, the total mass, and the total volume of the fuel cell and the pumps combined, respectively. As detailed in Table 1, the total mass and total volume were estimated by aggregating the corresponding values of two pumps, two fuel tanks, one DBHPFC, and one heater unit (power supply and temperature controller) (A, B, C, and D in Fig. 4). Because the same DBHPFC was used in all experiments, the high specific power and volumetric power density suggest that the pump system for a given produced electric power is lightweight and small-sized. The back work ratio, like the back work of turbine engines used to drive compressors in aircraft, indicates the amount of electrical power for pumping generated by the DBHPFC. Table 2 shows that the impedance pumping configuration not only reduced the volume and weight of the fuel cell systems, but also performed better than the peristaltic pumping configuration regarding the specific power, volumetric power density, and back work ratio.

Summary and Conclusions

Based on impedance pumping, a new valveless pump was successfully developed and applied to the fuel pumping of an all liquid-fueled direct borohydride–hydrogen peroxide fuel cell. The pump comprises a simple, quiet, economical, and energy-efficient actuation mechanism that combines a small DC motor, a cam, and an amber latex rubber tube, connected at both ends to rigid stainless-steel tubes with various acoustic impedances. At locations asymmetrical from the rigid ends, the net flow was generated by periodic compression of the pliable rubber tube to pump the fuel successfully. The pump flowrate was found to vary in a nonlinear manner with the actuation frequency, for a fixed actuation position ($x/L = 1/8$), waveform, duty cycle (36%), and input excitation amplitude ($\Delta y/D = 1$). The primary outcomes of this research are concluded as follows:

(1) The measured maximum flowrate of the impedance pump is 715 ml/min at the zero pump head at a motor actuation voltage range of 11–15 V (corresponding operation

frequency, 53–73 Hz). The flowrate achieves the optimal performance at an actuation frequency of 68 Hz.

(2) The variation in the flowrate with the actuation frequency for the fuel cell-connected scenario exhibits a trend that is broadly similar to that of the pump alone (Fig. 5). When the DBHPFC is connected to the impedance, the large head losses in the three-parallel-channel serpentine flow fields of the graphite bipolar plate can induce enormous diminution of the maximum pump flowrate to $Q = 30$ ml/min.

(3) Our DBHPFC successfully uses an alkaline borohydride aqueous solution (5 wt% $NaBH_4$ and 15 wt% NaOH) and an acid hydrogen peroxide aqueous solution (2.0 M H_2O_2 + 1.0 M H_2SO_4) as the liquid fuels for the anode and the cathode, respectively. The maximum power and current of about 13.0 W and 12.6 A were observed at anode and cathode flowrates of 30 ml/min.

(4) The combination of impedance pumps and the DBHPFC showed remarkable advantages in reducing the fuel cell system weight and volume while enhancing the specific power, volumetric power density, and back work ratio. In addition, the valveless characteristics of this pump are capable of preventing pump corrosion.

Impedance-based pumping provides an exciting new option for liquid fuel pumping systems. The feasibility of its application to pump fuel for liquid-fueled fuel cells is demonstrated by our experimental results. Although it is conceptually simple, further work is necessary to optimize its performance in practical applications, including (1) the proper choice of the flexible tube material to extend the pump life and reduce the resistance to friction from the compressing cam and (2) maximization of the impedance mismatch and flowrate accordingly. In addition, the optimal length of the flexible tube, the actuation frequency, and the position must be considered for the new combination of the impedance pump to expand the flowrate range. In the meanwhile, the stability of the Nafion membrane and the corresponding DBHPFC cell performance by pumping the basic fuel and the acid oxidant with valveless impedance pumps will be investigated.

Funding Data

- National Science Council (Grant No. NSC 99-2221-E-006-050-MY2; Funder ID: 10.13039/501100001868), Taiwan, the Republic of China.
- Research Grants Council, Hong Kong (Grant No. GRF 526913).

Nomenclature

f = actuation frequency, Hz
D = average diameter of the elastic tube, mm
H = water head, Pa
I = current, A
L = length of the elastic tube, mm
P = power, W
Q = flowrate, ml/min
R = flow resistance, Pa·min/ml
V = voltage, V
M_{total} = total mass of the fuel cell, kg
V_{total} = total volume of the fuel cell, m^3
E^0 = standard equilibrium cell voltage, V
x,y = coordinates

References

[1] Lux, S., Gu, L., Kopec, G., Bernas, R., and Miley, G., 2010, "Water Management Issues for Direct Borohydride/Peroxide Fuel Cells," ASME J. Fuel Cell Sci. Techol., **7**(2), p. 024501.

[2] Wen, C. Y., and Huang, G. W., 2008, "Application of a Thermally Conductive Pyrolytic Graphite Sheet to Thermal Management of a PEM Fuel Cell," J. Power Sources, **178**(1), pp. 132–140.

[3] Wen, C. Y., Lin, Y. S., and Lu, C. H., 2009, "Performance of a Proton Exchange Membrane Fuel Cell Stack with Thermally Conductive Pyrolytic Graphite Sheets for Thermal Management," J. Power Sources, **189**(2), pp. 1100–1105.

[4] Wen, C. Y., Lin, Y. S., Lu, C. H., and Luo, T. W., 2011, "Thermal Management of a Proton Exchange Membrane Fuel Cell Stack with Pyrolytic Graphite Sheets and Fans Combined," Int. J. Hydrogen Energy, **36**(10), pp. 6082–6089.

[5] Choudhury, N. A., Raman, R. K., Sampath, S., and Shukla, A. K., 2005, "An Alkaline Direct Borohydride Fuel Cell with Hydrogen Peroxide as Oxidant," J. Power Sources, **143**(1–2), pp. 1–8.

[6] Raman, R. K., and Shukla, A. K., 2006, "A Direct Borohydride/Hydrogen Peroxide Fuel Cell with Reduced Alkali Crossover," Fuel Cells, **7**(3), pp. 225–231.

[7] Miley, G. H., Luo, N., Mather, J., Burton, R., Hawkins, G., Gu, L., Byrd, E., Gimlin, R., Shrestha, P. J., Benavides, G., Laystrom, J., and Carroll, D., 2007, "Direct $NaBH_4/H_2O_2$ Fuel Cells," J. Power Sources, **165**(2), pp. 509–516.

[8] Cloutier, C. R., Alfantazi, A., and Gyenge, E., 2007, "Physicochemical Properties of Alkaline Aqueous Sodium Metaborate Solutions," ASME J. Fuel Cell Sci. Technol., **4**(1), pp. 88–98.

[9] Gu, L. F., Luo, N., and Miley, G. H., 2007, "Cathode Electro-Catalyst Selection and Deposition for a Direct Borohydride /Hydrogen Peroxide Fuel Cell," J. Power Sources, **173**(1), pp. 77–85.

[10] Luo, N., Miley, G. H., Kim, K. J., Burton, R., and Huang, X. Y., 2008, "NaBH4/H_2O_2 Fuel Cells for Air Independent Power Systems," J. Power Sources, **185**(2), pp. 685–690.

[11] Liu, B. H., and Li, Z. P., 2009, "Current Status and Progress of Direct Borohydride Fuel Cell Technology Development," J. Power Sources, **187**(2), pp. 291–297.

[12] Wen, C. Y., and Chang, H. T., 2009, "Design and Characterization of Valveless Impedance Pumps," J. Mech., **25**(4), pp. 345–354.

[13] Rinderknecht, D., Hickerson, A. I., and Gharib, M., 2005, "A Valveless Micro Impedance Pump Driven by Electromagnetic Actuation," J. Micromech. Microeng., **15**(4), pp. 861–866.

[14] Hickerson, A. I., Rinderknecht, D., and Gharib, M., 2005, "Experimental Study of the Behaviors of a Valveless Impedance Pump," Exp. Fluids, **38**(4), pp. 535–540.

[15] Hickerson, A. I., and Gharib, M., 2006, "On the Resonance of a Pliant Tube as a Mechanism for Valveless Pumping," J. Fluid Mech., **555**, pp. 141–148.

[16] Wen, C. Y., Yeh, S. J., Leong, K. P., Kuo, W. S., and Lin, H., 2013, "Application of a Valveless Impedance Pump in a Liquid Cooling System," IEEE Trans. Components Packag. Manuf. Technol., **3**(5), pp. 783–791.

[17] Chang, H. T., Lee, C. Y., and Wen, C. Y., 2007, "Design and Modeling of Electromagnetic Actuator in MEMS-Based Valveless Impedance Pump," Microsyst. Technol., **13**(11–12), pp. 1615–1622.

[18] Chang, H. T., Lee, C. Y., Wen, C. Y., and Hong, B. S., 2007, "Theoretical Analysis and Optimization of Electromagnetic Actuation in a Valveless Micro Impedance Pump," Microelectron. J., **38**(6–7), pp. 791–799.

[19] Lee, C. Y., Chang, H. T., and Wen, C. Y., 2008, "A MEMS Based Valveless Impedance Pump Utilizing Electro-Magnetic Actuation," J. Micromech. Microeng., **18**(3), p. 035044.

[20] Chang, H. T., Wen, C. Y., and Lee, C. Y., 2009, "Design, Analysis and Optimization of an Electromagnetic Actuator for a Micro Impedance Pump," J. Micromech. Microeng., **19**(8), p. 085026.

[21] Lee, C. Y., Chen, Z. H., Chang, H. T., Wen, C. Y., and Cheng, C. H., 2009, "Design and Fabrication of Novel Micro Electromagnetic Actuator," Microsyst. Technol., **15**(8), pp. 1171–1175.

[22] Wen, C. Y., Cheng, C. H., Jian, C. N., Nguyen, T. A., Hsu, C. Y., and Su, Y. R., 2006, "A Valveless Micro Impedance Pump Driven by PZT Actuation," Mater. Sci. Forum, **505–507**, pp. 127–132.

[23] Liebau, G., 1954, "Arterielle Pulsation und Venöse Vepulsation," Z. Gesamte Exp. Med., **123**(1), pp. 71–90.

[24] Liebau, G., 1955, "Prinzipien Kombinierter Ventilloser Pumpen, Abgeleitet Vom Menschlichen Blutkreislauf," Naturwissenschaften, **42**(1), pp. 339–345.

[25] Thomann, H., 1978, "A Simple Pumping Mechanism in a Valveless Tube," Z. Angew. Math. Phys., **29**(2), pp. 169–177.

[26] Moser, M., Huang, J. W., Schwarz, G. S., Kenner, T., and Noordergraaf, A., 1998, "Impedance Defined Flow: Generalization of William Harvey's Concept of the Circulation—370 Years Later," Int. J. Cardiovasc. Med. Sci., **1**(3/4), pp. 205–211.

[27] Jung, E., and Peskin, C., 2001, "Two-Dimensional Simulations of Valveless Pumping Using Immersed Boundary Methods," SIAM J. Sci. Compu., **23**(1), pp. 19–45.

[28] Borzì, A., and Propst, G., 2003, "Numerical Investigation of the Liebau Phenomenon," Z. Angew. Math. Phys., **54**(6), pp. 1050–1072.

[29] Ottensen, J. T., 2003, "Valveless Pumping in a Fluid-Filled Closed Elastic Tube System: One Dimensional Theory with Experimental Validation," J. Math. Biol., **46**(4), pp. 309–332.

[30] Auerbach, D., Moehring, W., and Moser, M., 2004, "An Analytic Approach to the Liebau Problem of Valveless Pumping," Cardiovasc. Eng., **4**(2), pp. 201–207.

[31] Manopoulos, C. G., Mathioulakis, D. S., and Tsangaris, S. G., 2006, "One-dimensional Model of Valveless Pumping in a Closed Loop and a Numerical Solution," Phys. Fluids, **18**(1), p. 017106.

[32] Huang, X. Y., Wen, C. Y., and Jiao, Z. J., 2010, "A Standing Wave Model for Acoustic Pumping Effect in Microchannels," Appl.Acoust., **71**(2), pp. 164–168.

[33] Li, Z. P., Liu, B. H., Zhu, J. K., and Suda, S., 2006, "Depression of Hydrogen Evolution During Operation of a Direct Borohydride Fuel Cell," J. Power Sources, **163**(1), pp. 555–559.